Applied Catalysis B: Environmental 303 (2022) 120879

Contents lists available at ScienceDirect

Applied Catalysis B: Environmental

journal homepage: www.elsevier.com/locate/apcatb

Facile synthesis of MoP-Ru_2P on porous N, P co-doped carbon for efficiently electrocatalytic hydrogen evolution reaction in full pH range

Yuxiao Gao [a], Zhi Chen [a], Ying Zhao [a], Wenli Yu [a], Xianliang Jiang [a], Maoshuai He [a], Zhenjiang Li [b], Tianyi Ma [c], Zexing Wu [a,*], Lei Wang [a,*]

[a] Key Laboratory of Eco-chemical Engineering, Taishan Scholar Advantage and Characteristic Discipline Team of Eco Chemical Process and Technology, Ministry of Education, Laboratory of Inorganic Synthesis and Applied Chemistry, College of Chemistry and Molecular Engineering, Qingdao University of Science and Technology, Qingdao 266042, PR China

[b] College of Materials Science and Engineering, College of Electromechanical Engineering, Key Laboratory of Polymer Material Advanced Manufacturing's Technology of Shandong Province, Qingdao University of Science and Technology, Qingdao, Shandong Province 266061, PR China

[c] Centre for Translational Atomaterials, Swinburne University of Technology, John Street, Hawthorn, VIC 3122, Australia

ARTICLE INFO

Keywords:
Metal phosphides
Electrocatalysts
Hydrogen evolution reaction
Water-splitting
Porous structure

ABSTRACT

Developing efficient, novel and pH-universal electrocatalysts toward hydrogen evolution reaction (HER) is a challenging and meaningful task for the large-scale and practical hydrogen application via electrocatalytic overall water-splitting. Herein, we propose one-pot strategy to prepare MoP and Ru_2P nanoparticles supported on N, P co-doped carbon (MoP-Ru_2P/NPC) with porous nanostructures. Benefiting from overly specific characters, the synthetical MoP-Ru_2P/NPC displays low overpotentials of 47 mV, 126 mV and 82 mV to obtain 10 mA cm^{-2} in alkaline, neutral and acid electrolytes as well as remarkable stability. Moreover, a low cell voltage (1.49 V) is required to spur 10 mA cm^{-2} for full water-splitting in 1 M KOH with the MoP-Ru_2P/NPC and commercial NiFe foam as the cathode and anode, respectively. Remarkably, the intermittent sustainable energies, including wind, solar and thermal energies, can drive hydrogen generation directly and then stored them accordingly.

1. Introduction

Hydrogen, with high-energy density and carbon-free merits, is considered as promising energy to replace traditional fossil fuels [1–7]. Electrocatalytic water-splitting for hydrogen generation provides an ideal approach to alleviate the pressing environmental pollution and energy crisis, especially when it drived by the sustainable and intermittent energies such as thermal energies, wind and solar [8–15]. Whereas, the sluggish reaction kinetics of hydrogen evolution reaction (HER) limits the catalytic efficiency of water electrolysis technology and then increased the electricity consumption [16–20]. To settle the above issue, Pt based nanomaterials are generally required to accelerate the reaction kinetics which own excellent intrinsic activity with small overpotential and low Tafel slope in acid media [21–27]. However, the high cost and scarcity hindered their large scale applications toward hydrogen economy. Therefore, tremendous efforts are devoted to explore non-Pt electrocatalysts to overcome the energy barriers of HER [28,29].

In the past decades, enormous endeavors are dedicated to the investigation on transition metals based nanomaterials, such as metal nitride, metal phosphide, metal sulfide and metal carbide for HER, owing to their abundant resources [30–34]. Among them, transition metal phosphides (TMPs) have attracted tremendous attentions due to their excellent essential catalytic activity and superior long-time stability [35–46]. Despite these considerable advancements, the catalytic performances of TMPs are still unsatisfactory compare with Pt-related nanomaterials. Recently, Ru, as an promising alternative to Pt, is deemed as an ideal electrocatalyst toward HER due to the similar bond strength to hydrogen and its 4% price of Pt [47–50]. Nevertheless, Ru based nanomaterials also confront higher cost compare with the transition metals. It is discovered that the introduced phosphorous (P) into Ru to form Ru-based phosphide, such as RuP, Ru_2P, RuP_2, is a valid approach to enhance the catalytic activity by altering the physicochemical property of Ru [51]. In general, the loading of Ru species is high in order to achieve excellent electrocatalytic performance and then enhanced the cost of the design electrocatalyst [52]. As reported, the binary transition metal phosphides with various chemical and structural superiorities could improve the electrocatalytic performance effectively

* Correspondence to: Qingdao University of Science and Technology, Qingdao 266042, PR China.
E-mail addresses: splswzx@qust.edu.cn (Z. Wu), inorchemwl@126.com (L. Wang).

https://doi.org/10.1016/j.apcatb.2021.120879
Received 25 August 2021; Received in revised form 16 October 2021; Accepted 28 October 2021
Available online 2 November 2021

[53,54]. For instance, Che and co-authors synthesized Ni_2P-Co_2P network on flexible carbon cloth and it presented wonderful electrocatalytic property toward HER in alkaline and acid media [55]. Except to construct heterogeneous bimetallic phosphides, anchored the metal phosphides onto the carbon matrix is considered as a valid approach to boost the catalytic activity. For example, Li and co-authors anchored ruthenium phosphide onto three dimensional hollow graphene nanospheres and it exhibited small overpotentials in wide pH range [56].

As a proof-of-concept study, here, heterogeneous bimetallic phosphide supported on N, P co-codoped carbon (MoP-Ru_2P/NPC) was reported using low toxic and resourceful melamine phosphate and glucose as the N, P and C precursor (Scheme 1). The coupling effects between MoP and Ru_2P induced promoting the catalytic performance effectively. Moreover, the addition of glucose also plays a vital role on promoting the electrocatalytic activity by avoiding the aggregation of nanoparticles and then exposing more active sites. The as-synthesized MoP-Ru_2P/NPC electrocatalyst exhibit wonderful electrocatalytic property for HER in full pH values with low content of Ru. Moreover, the obtained bimetallic phosphides also own remarkable long-term stability in various harsh electrolytes. Interestingly, the intermittent sustainable energies can be stored into hydrogen energy by driving overall water-splitting with the designed MoP-Ru_2P/NPC and commercial as both cathode and anode.

2. Experimental section

2.1. Materials

Melamine phosphate (MP), Molybdenum chloride ($MoCl_5$), Ruthenium (III) chloride anhydrous ($RuCl_3$), D-(+)-glucose ($C_6H_{12}O_6$).

2.2. Synthesis of MoP-Ru_2P/NPC

For the preparation of MoP-Ru_2P/NPC, 0.2241 g of MP, 0.0455 g of $MoCl_5$, 0.9 g of $C_6H_{12}O_6$ and 6 mg $RuCl_3$ were dissolved in 20 mL of ultra-pure water, and then the mixture was heated at 75 °C to obtain gel like precursor. Finally, the precursor was annealed in Ar atmosphere with 10 ℃/min to 900 ℃.

2.3. Physical characterization

The morphology of the catalysts was characterized by scanning electron microscopy (SEM) and transmission electron microscopy (TEM). The crystal constructions of the prepared electrocatalysts were researched by X-ray diffraction (XRD). The elemental components of the catalysts was studied by X-ray photoelectron spectroscopy (XPS).

2.4. Electrochemical measurements

Using electrochemical workstation of CHI-760E to test performance in 1 M KOH, 0.5 M H_2SO_4, and 1 M PBS, reversible hydrogen electrode as a reference electrode. Cyclic voltammetry and linear sweeping voltammograms (LSVs) were researched at 5 mV s^{-1} with 95% iR-corrected. For RHE, filling the electrode with different electrolytes (1 M KOH, 0.5 M H_2SO_4 or 1 M PBS), and then perform I-t chronoamperometric measurement at 10 V with different time.

3. Results and discussions

3.1. Morphology and structure characterizations

Transmission electron microscopy (TEM) measurements and scanning electron microscopy (SEM) were conducted to study the nanostructure of the as-synthesized electrocatalysts. Obviously, the prepared MoP exhibits aggregated nanoparticles and then limited the amounts of exposed active sites. However, MoP-Ru_2P/NPC presents porous nanosheets morphology after the instruction of glucose (Fig. S1). The specific nanostructure provides lots of active sites during electrocatalytic process. The TEM (Fig. 1a, b) images also confirm the porous morphology with rich pores. As shown in Fig. 1c, the HR-TEM image of MoP-Ru_2P/NPC illustrates lattice spacing of 0.31 nm and 0.21 nm, corresponding to the plane of MoP (002) and Ru_2P (210), respectively. Moreover, the generated interfaces (red dotted line) also favor on promoting the electrocatalytic performances by optimizing the reaction kinetics. The scanning TEM (STEM) image (Fig. 1d) and EDX results (Fig. 1e–i, S2) revealed that Mo, Ru, N, P and C elements are uniformly spread over the synthesized MoP-Ru_2P/NPC.

The crystal structure of the obtained electrocatalysts were investigated by XRD. The XRD pattern of MoP maintained well before and after the introduction of glucose, but the grain size decreased owing to the aggregation avoided during pyrolysis process (Fig. S3a, b). As shown in Fig. 2a, the prepared MoP-Ru_2P/NPC is composed by MoP (PDF# 24-0771) and Ru_2P (PDF# 65-2382). Fig. S3c verifies that Ru_2P/NPC is mainly composed by Ru_2P (PDF# 65-2382) and the XRD pattern of NPC demonstrates its amorphous property (Fig. S3d). And the ICP indicates the content of Ru is only10 *wt*%. Raman spectrum exhibits two characteristic bands at ~ 1345 and ~ 1583 cm^{-1} are ascribed to the disordered carbon (D) and graphitic carbon (G) bands, demonstrating the existence of carbon support (Fig. 2b). In addition, the specific surface area and porous structure of as-prepared MoP-Ru_2P/NPC was confirmed by nitrogen adsorption-desorption isotherm (Fig. 2c, d). As expected, the synthesized MoP-Ru_2P/NPC possesses large specific surface area of 134.95 m^2/g. Moreover, the pore size distribution curve demonstrates the mesoporous pores in MoP-Ru_2P/NPC (Fig. 2d). As expected, the designed electrocatalyst with big specific surface area with mesopores

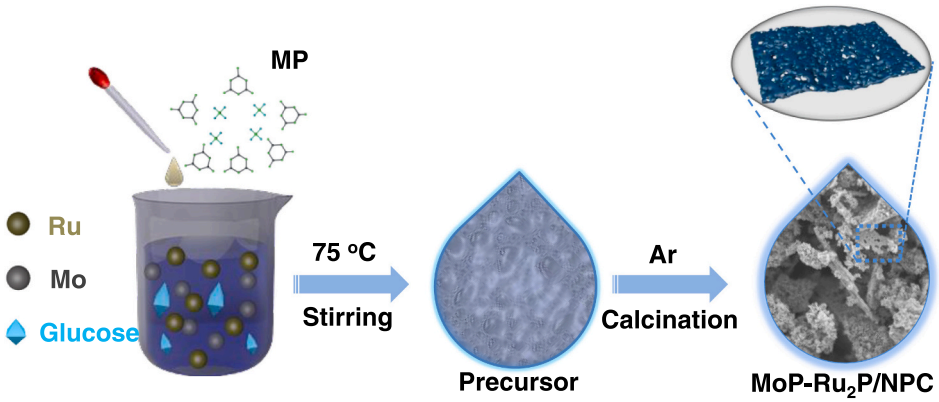

Scheme 1. Schematic illustration of the synthetic procedure of MoP-Ru_2P/NPC.

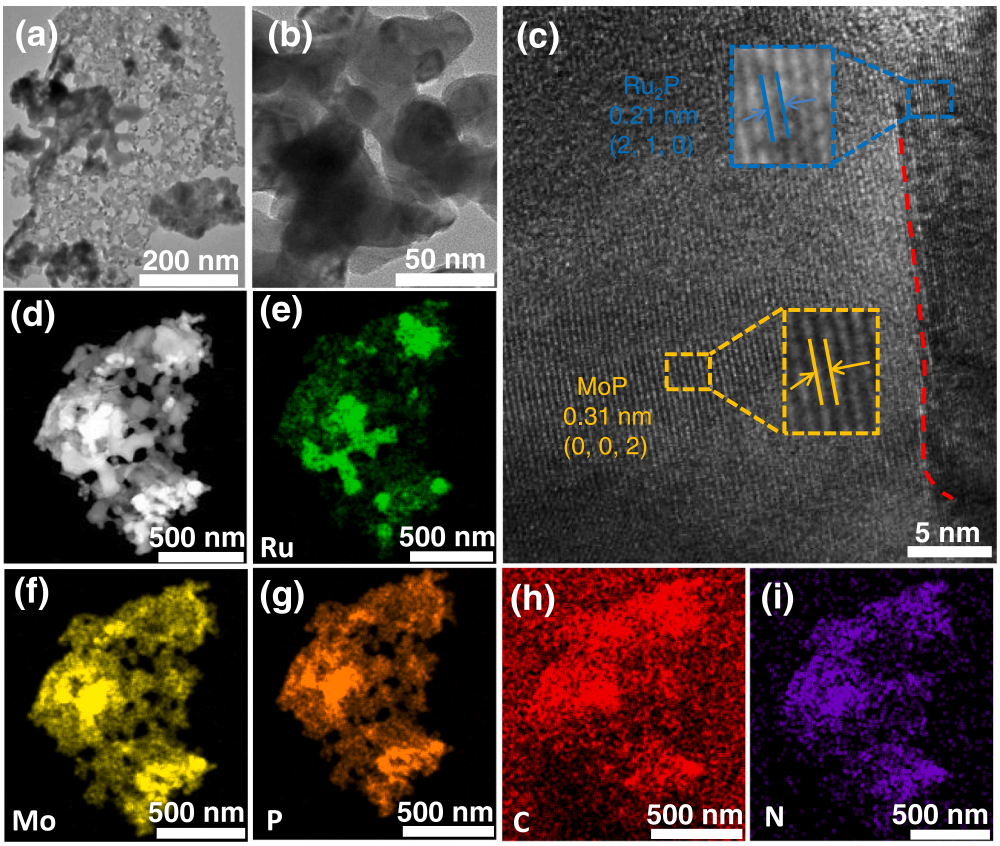

Fig. 1. Low (a and b) and high resolution (c) TEM images of MoP-Ru_2P/NPC. (d) The scanning TEM (STEM) image of MoP-Ru_2P/NPC. EDX elemental mappings of Ru (e), Mo (f), P (g), C (h), N (i) in MoP-Ru_2P/NPC.

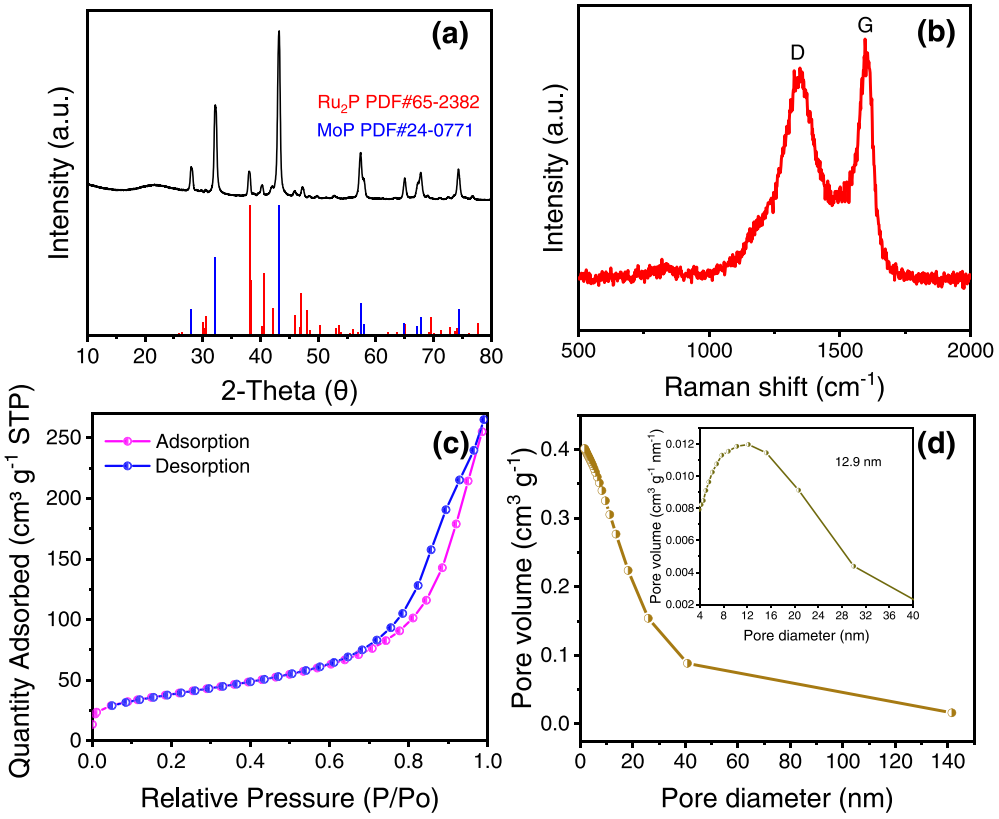

Fig. 2. XRD patterns (a) and Raman spectra (b) of MoP-Ru_2P/NPC. N_2 adsorption/desorption isotherm (c) and pore size distribution (d) of MoP-Ru_2P/NPC.

would expose abundant active sites, favor the transport of electrolyte, accelerate the release of generated gas bubbles and mass transport, thus improving the electrocatalytic activity effectively.

X-ray Photoelectron spectroscopy (XPS) was applied to analyze the composition and chemical valence of the prepared electrocatalysts. In accordance with the elemental images, the elements of Ru, Mo, C, N, and P is observed in the XPS survey spectrum of MoP-Ru_2P/NPC (Fig. 3a). Moreover, the elements of C, N, Mo, and P (Fig. S4a) and C, N, Ru, P are observed in MoP/NPC and RuP_2/NPC, respectively (Fig. S5a). The C 1s XPS spectra (Fig. 3b) can be fitted into three peaks of 284.8, 286.3, and 289.1 eV [57,58], corresponding to the C-C, C-P/N, C-O bonds, and another peak of 279.9 eV corresponding to Ru (near the C 1s peak). For P 2p, the doublet at around 129.3 eV/130.2 eV is assigned to the metal-P bond and the peak of P-O is located 133.6 eV (Fig. 3c and Figs. S4, 5b) [59–62]. While the peaks of N 1s (Fig. 3d) in MoP-Ru_2P/NPC are located at 394.3 (Mo 3p), 395.7 and 397.6 (N-C), 399.4 (pyridinic-N), 400.6 (pyrrolic-N), 401.7 eV (graphitic-N) [63]. The deconvolution of the core-level Mo 3d XPS spectrum (Fig. 3e) shows three pairs of peaks, corresponding to the Mo^{3+}, Mo^{4+}, Mo^{6+} that is similar to the MoP/NPC (Fig. S4c). The peaks of Ru 3p are located at 461.4, 483.7 eV in MoP-Ru_2P/NPC, assigning to Ru $3p_{3/2}$ and Ru $3p_{1/2}$ (Fig. 3f and Fig. S5c) [64].

3.2. Electrochemical measurement

The electrocatalytic performances of all the designed samples, including commercial Pt/C, were conducted with a conventional three-electrode setup. Fig. 4a displays the linear sweep voltammetry (LSV) curves of MoP-Ru_2P/NPC, MoP/NPC, Ru_2P/NPC, MoP, NPC and Pt/C in 1 M KOH. As can be seen in Fig. 4a, MoP-Ru_2P/NPC outperform all the investigated samples, with the smallest overpotential of 47 mV to drive 10 mA cm^{-2}. In contrast, Pt/C, MoP/NPC, Ru_2P/NPC, MoP and NPC require overpotentials of 55 mV, 163 mV, 404 mV, 217 mV and 339 mV to reach the identical electric density. Moreover, MoP-Ru_2P/NPC achieves the highest current density with the same applied overpotentials (Fig. 4b) and then further confirmed its excellent electrocatalytic activity for HER. In addition, the molar ratio of MP and Mo was also investigated. As illustrated in Fig. S6, the molar ratio with 6-1 presents outstanding electrocatalytic activity (217 mV@10 mA cm^{-2}) relative to 3-1 (262 mV@10 mA cm^{-2}) and 9-1 (265 mV@10 mA cm^{-2}). We also investigated the effects of glucose (G) and Ru contents on regulating the electrocatalytic activities. The results demonstrate that the addition of G and Ru decreased the overpotentials evidently (Fig. S7). Fig. 4c illustrates the corresponding Tafel slopes. Obviously, the Tafel slope of MoP-Ru_2P/NPC is 36.93 mV dec^{-1}, and it is smaller than Pt/C (44.69 mV dec^{-1}), MoP/NPC (56.34 mV dec^{-1}), MoP (56.13 mV dec^{-1}) and Ru_2P/NPC (199.39 mV dec^{-1}), proving the favorable reaction kinetics of the designed MoP-Ru_2P/NPC. In accordance with the order of electrocatalytic performance, MoP-Ru_2P/NPC shows the value of 40.17 mF cm^{-2}, which is larger than MoP/NPC (15.48 mF cm^{-2}), MoP (3.22 mF cm^{-2}), Ru_2P/NPC (0.64 mF cm^{-2}) and NPC (0.63 mF cm^{-2}), demonstrating more active sites exposed of the developed MoP-Ru_2P/NPC (Fig. 4d). Noticeably, the as-synthetic MoP-Ru_2P/NPC possesses lower overpotential and smaller Tafel slope compare with some of reported values (Fig. 4e and Table S1). Electrochemical double layer capacitance (C_{dl}) was obtained by cyclic voltammetry (CV) at different scan rates from 20 mV s^{-1} to 120 mV s^{-1} (Fig. S8). With regard to stability, the chronoamperometry measurement indicates that the current density presents negligible attenuation over period of 12 h, indicating its superior stability for HER in alkaline media (Fig. 4f).

The HER activity in neutral electrolyte also plays significant role on the practical overall water-splitting. Then, the electrocatalytic properties of the developed electrocatalysts were also evaluated in 1 M PBS. As shown in Fig. 5a, the designed MoP-Ru_2P/NPC also owns the smallest overpotential (126 mV@10 mA cm^{-2}), except Pt/C, relative to MoP/NPC (179 mV@10 mA cm^{-2}), MoP (227 mV@10 mA cm^{-2}). However, the current density of MoP-Ru_2P/NPC surpasses Pt/C with the applied potential over 0.2 V. Moreover, MoP-Ru_2P/NPC achieves the highest current density with the same applied overpotentials (Fig. 5b). Fig. 5c illustrates the derived Tafel slopes from the LSVs. Obviously, the corresponding Tafel slope of MoP-Ru_2P/NPC is 70.89 mV dec^{-1}, lower than those of MoP/NPC (89.19 mV dec^{-1}) and MoP (82.92 mV dec^{-1}). The calculated C_{dl} demonstrates that MoP-Ru_2P/NPC delivers the largest value of 29.38 mF cm^{-2}, indicating its more rich exposed electrocatalytic active sites (Fig. 5d). Impressively, the performance of MoP-Ru_2P/NPC is also superior to some recently values in neutral electrolyte

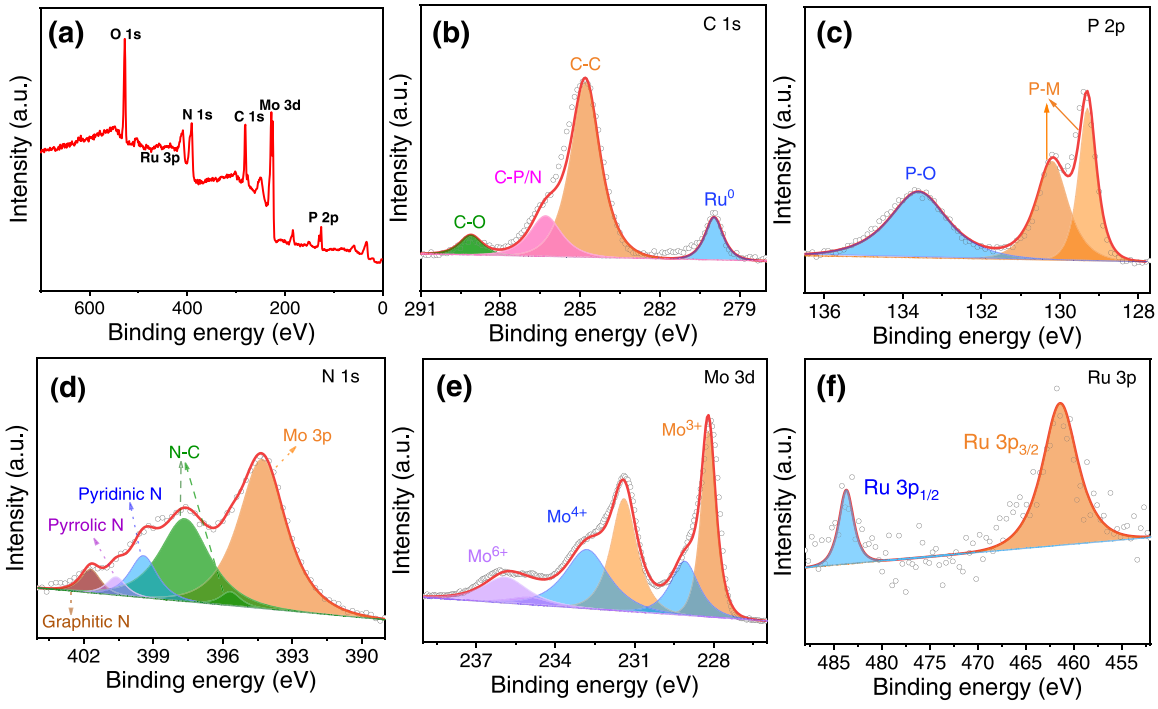

Fig. 3. Survey spectrum (a) and high-resolution XPS spectra of (b) C 1s, (c) P 2p, (d) N 1s (e) Mo 3d and Ru 3p (f) for MoP-Ru_2P/NPC.

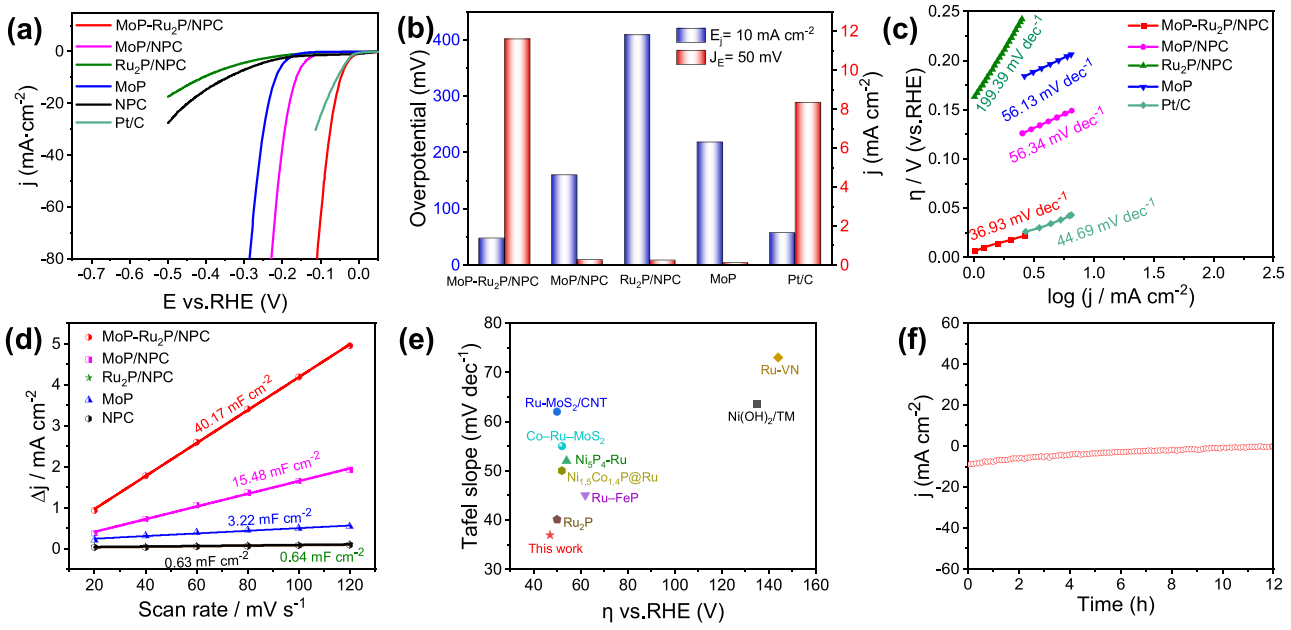

Fig. 4. (a) LSVs of MoP-Ru_2P/NPC, MoP/NPC, Ru_2P/NPC, MoP, NPC and Pt/C for HER in 1 M KOH. (b) Comparison of overpotentials and current densities of the samples. (c) Tafel slopes of the investigated electrocatalysts. (d) Double layer capacitance plots of the researched samples. (e) Comparison of the electrocatalytic performance with reported catalysts. (f) Stability test of MoP-Ru_2P/NPC for 12 h under 10 mA cm^{-2}.

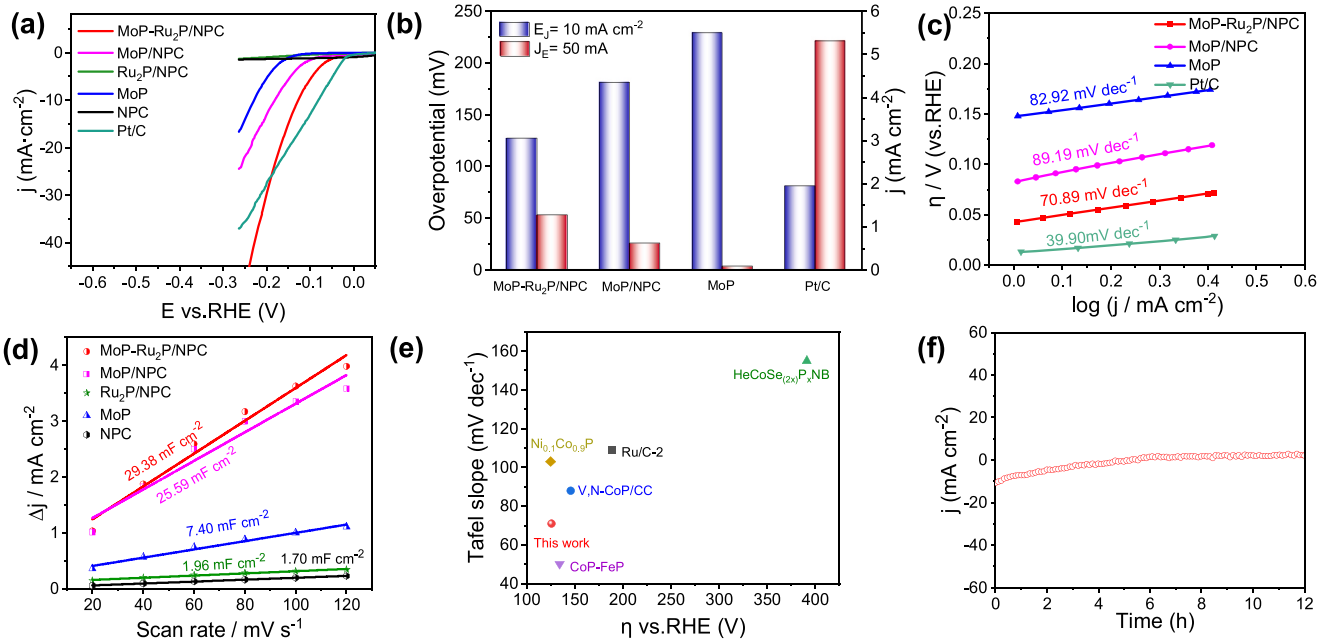

Fig. 5. (a) LSVs of MoP-Ru_2P/NPC, MoP/NPC, Ru_2P/NPC, MoP, NPC and Pt/C for HER in 1 M PBS. (b) Related overpotentials and current densities of the researched samples. (c) Corresponding Tafel slopes of the studied electrocatalysts. (d) Double layer capacitance plots of the researched samples. (e) Comparison of the electrocatalytic performance with reported catalysts. (f) Stability test of MoP-Ru_2P/NPC for 12 h under 10 mA cm^{-2}.

(Fig. 5e and Table S2). In addition, the electrocatalytic properties also can be optimized by tuning the contents of Mo, Ru and G in the synthesized electrocatalysts (Fig. S9). Meanwhile, the time-dependent current density curve of MoP-Ru_2P/NPC without obvious decay as long as 12 h proves the good stability in 1 M PBS (Fig. 5f).

As discussed above, the synthesized MoP-Ru_2P/NPC exhibits excellent electrocatalytic performance toward HER in proton free electrolytes. Then, we investigated the catalytic properties of the as-obtained nanomaterials in acid medium. It can be clearly observed that MoP-Ru_2P/NPC owns the smallest overpotential (82 mV@10 mA cm^{-2}) and lowest Tafel slope (64.99 mV dec^{-1}), except Pt/C, relative to the control samples (Fig. 6a, b). Specially, the MoP-Ru_2P/NPC obtains the largest current density of 3.37 mA cm^{-2} at 50 mV compared with MoP/NPC (0.34 mA cm^{-2}), Ru_2P/NPC (0.52 mA cm^{-2}) and MoP (0.09 mA cm^{-2}), confirming its superior catalytic activity further (Fig. 6c). The excellent catalytic activity of MoP-Ru_2P/NPC can be ascribed to the abundant exposed active sites, determined by the measured C_{dl}, and then accelerate then catalytic process (Fig. 6d). Except the remarkable catalytic performance, the prepared MoP-Ru_2P/NPC also possesses outstanding long-term stability in acid electrolyte (Fig. 6e). Impressively, the

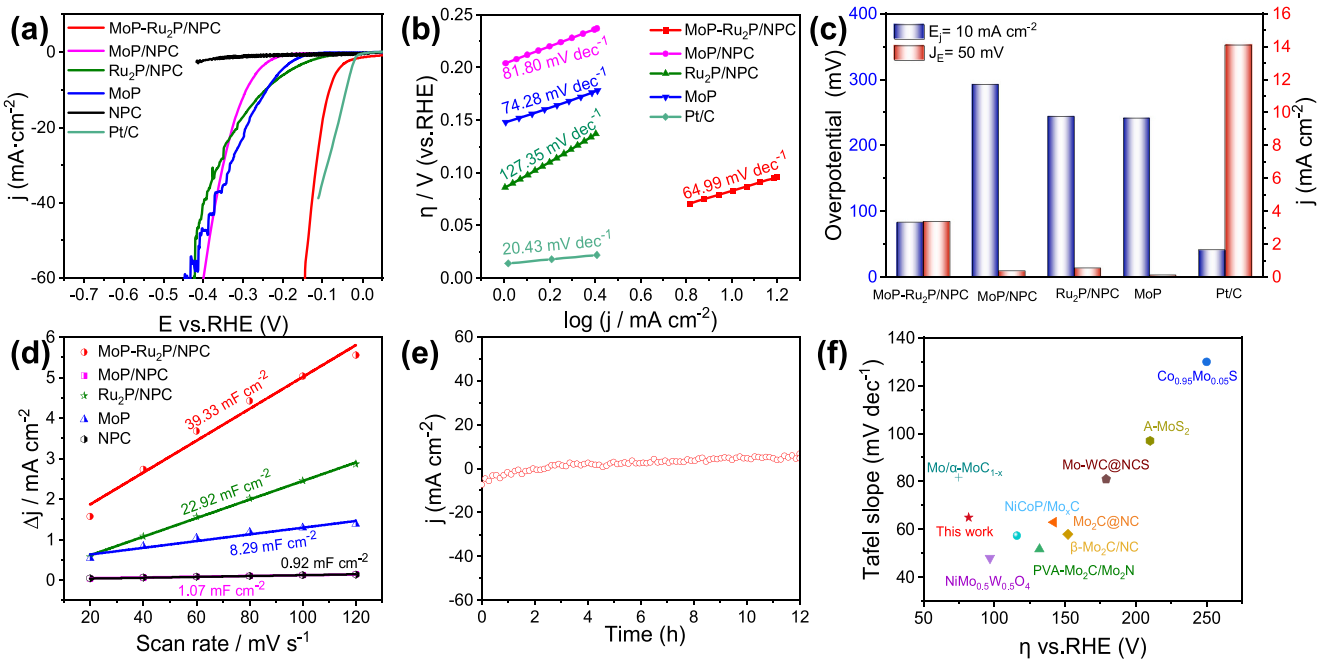

Fig. 6. LSVs of MoP-Ru_2P/NPC, MoP/NPC, Ru_2P/NPC, MoP, NPC and Pt/C for HER in 0.5 M H_2SO_4 (a) and corresponding Tafel slopes (b). (c) Related overpotentials and current densities of the researched samples. (d) Double layer capacitance plots of the researched samples. (e) Stability test of MoP-Ru_2P/NPC for 12 h under 10 mA cm^{-2}. (f) Comparison of the electrocatalytic performance with reported catalysts.

performance of MoP-Ru_2P/NPC is also superior to some recently values in acid electrolyte (Fig. 6f and Table S3). Similarly, the catalytic performances also can be regulated by altering the contents of Mo, Ru and G in the prepared electrocatalysts (Fig. S10).

Encouraged by the excellent electrocatalytic performance toward HER in alkaline media, a two-electrode alkaline setup was fabricated by using MoP-Ru_2P/NPC and commercial as the cathode and anode, respectively. As reference, Pt/C || RuO_2 is also assembled into a two-electrode configuration for overall water splitting. As shown in Fig. 7a, the electrolyzer of NiFe || MoP-Ru_2P/NPC-NiFe only needs a small cell voltage of 1.49 V to achieve the current density of 10 mA cm^{-2} for full water-splitting relative to the value of 1.63 V for the most advanced RuO_2|| Pt/C. All in all, the activity showing in the electrolyzer of NiFe || MoP-Ru_2P/NPC-NiFe is comparable with some recently published works (Table S4). As illustrated in Fig. 7b, the NiFe || MoP-Ru_2P/NPC-NiFe shows superior long-term stability with negligible

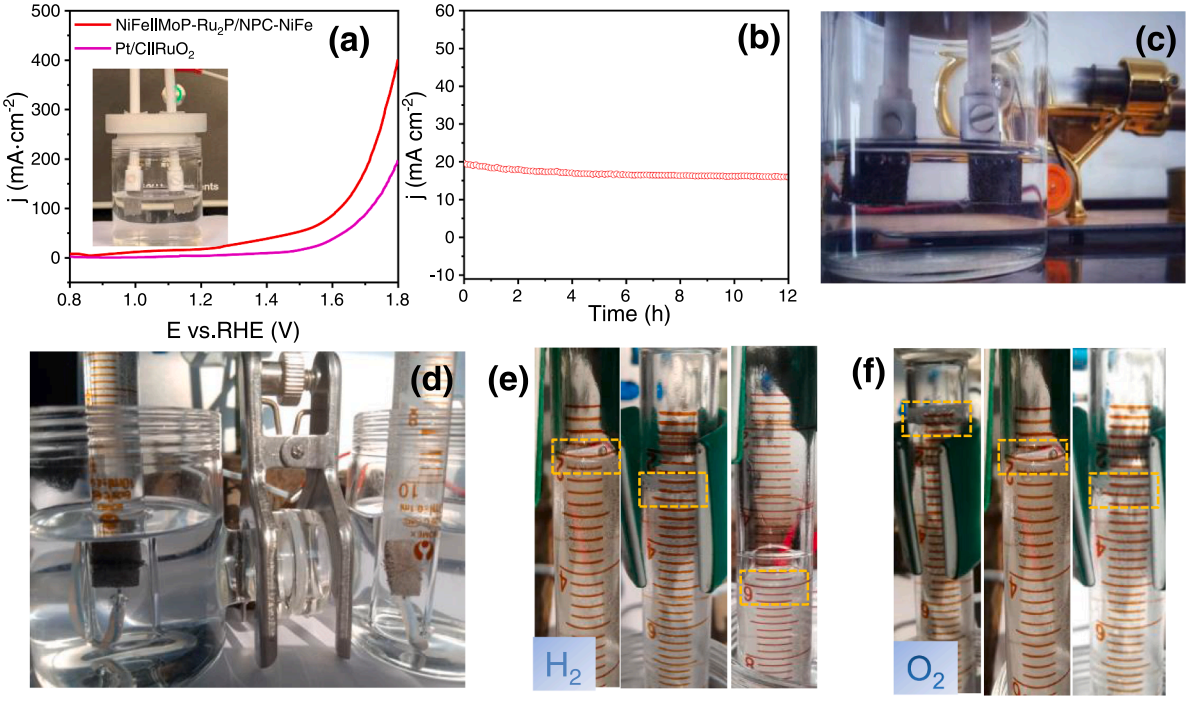

Fig. 7. (a) Full water-splitting in 1 M KOH of the designed electrocatalyst and the reference sample. (b) Chronopotentiometric curve of MoP-Ru_2P/NPC for 12 h. (c) The MoP-Ru_2P/NPC || NiFe electrolyzer is driven by Stirling engine. (d) Quantitative measurement of the amount of oxygen and hydrogen by the bubble extraction method. Photographs of hydrogen (e) and oxygen (f) and collected at various reaction time.

current density attenuation over 12 h at 10 mA cm^{-2}. As shown in Fig. 7c and Movie S1, we used the Stirling engine to drive overall water-splitting. Evidently, sumless gas bubbles generated on the two electrodes upon the sustainable energies input, demonstrating the promising practical applications on storing the intermittent energies (Fig. 7d–f). To further assess the feasibility for energy storage, we adopted intermittent energies, including wind energy, solar energy to drive overall water-splitting (Fig. S11a, b and Movie S2, 3). Impressively, a single AAA cell with a voltage of 1.5 V can drive the full water splitting with many bubbles produced on both anode and cathode, demonstrating the high catalytic efficiency of the prepared electrocatalyst (Fig. S11c and Movie S4).

Supplementary material related to this article can be found online at doi:10.1016/j.apcatb.2021.120879.

Supplementary material related to this article can be found online at doi:10.1016/j.apcatb.2021.120879.

Supplementary material related to this article can be found online at doi:10.1016/j.apcatb.2021.120879.

Supplementary material related to this article can be found online at doi:10.1016/j.apcatb.2021.120879.

4. Conclusion

In summary, highly-efficient and robust MoP-Ru_2P/NPC electrocatalyst has been successfully prepared via a straightforward one-pot avenue with the low-toxic and resourceful melamine phosphate and glucose as the N, P and C resources. The as-synthesized MoP-Ru_2P/NPC shows wonderful electrocatalytic activities for HER in full pH values. The electrocatalyst also owns impressive long-term stability in various harsh electrolytes. In addition, a two-electrode setup, with the MoP-Ru_2P/NPC and commercial NiFe foam as the cathode and anode, respectively, is assembled to drive overall water-splitting in alkaline media with a small potential of 1.49 V to achieve 10 mA cm^{-2}. Remarkably, various sustainable energies, including solar, wind and thermal energies, can be utilized to drive the water-splitting effectively. This facile and eco-friendly synthetic avenue can effectively boost the exploitation of efficient and durable electrocatalysts toward scalable hydrogen production.

CRediT authorship contribution statement

Yuxiao Gao: Conceptualization, Verification, Formal analysis, Data curation, Writing – original draft. **Zhi Chen:** Data curation, Methodology. **Ying Zhao:** Data curation, Software, Formal analysis. **Wenli Yu:** Data curation, Writing. **Xianliang Jiang:** Data curation. **Maoshuai He:** Investigation. **Zhenjiang Li:** Data curation. **Tianyi Ma:** Data curation, Supervision. **Zexing Wu:** Funding acquisition, Supervision. **Lei Wang:** Funding acquisition, Supervision.

Declaration of Competing Interest

The authors declare that they have no known competing financial interests or personal relationships that could have appeared to influence the work reported in this paper.

Acknowledgement

The authors acknowledge funding support from the National Natural Science Foundation of China (22002068; 51772162, and 52072197), Project funded by China Postdoctoral Science Foundation (2021M691700); Youth Innovation and Technology Foundation of Shandong Higher Education Institutions, China (2019KJC004), Outstanding Youth Foundation of Shandong Province, China (ZR2019JQ14), Taishan Scholar Young Talent Program (tsqn201909114), Major Scientific and Technological Innovation Project (2019JZZY020405), and Major Basic Research Program of Natural Science Foundation of Shandong Province under Grant No. ZR2020ZD09. The Natural Science Foundation of Shandong Province of China (ZR2019BB002; ZR2018BB031), Australian Research Council (ARC) Future Fellowship (FT210100298), CSIRO Energy Centre, and the Victorian Government's support through the provision of a grant from veski – Study Melbourne Research Partnerships (SMRP) project.

Appendix A. Supporting information

Supplementary data associated with this article can be found in the online version at doi:10.1016/j.apcatb.2021.120879.

References

[1] S. Geng, Y. Liu, Y.S. Yu, W. Yang, H. Li, Engineering defects and adjusting electronic structure on S doped MoO_2 nanosheets toward highly active hydrogen evolution reaction, Nano Res. 13 (2019) 121–126.

[2] G. Zhao, W. Ma, X. Wang, Y. Xing, S. Hao, X. Xu. Self-water-absorption-type two-dimensional composite photocatalyst with high-efficiency water absorption and overall water-splitting performance, Adv. Powder Mater. ⟨https://doi.org/10.1016/j.apmate.2021.09.008⟩.

[3] A. Majeed, X. Li, P.-X. Hou, H. Tabassum, L. Zhang, C. Liu, H.-M. Cheng, Monolayer carbon-encapsulated Mo-doped Ni nanoparticles anchored on single-wall carbon nanotube film for total water splitting, Appl. Catal. B: Environ. 269 (2020), 118823.

[4] M. Qu, Y. Jiang, M. Yang, S. Liu, Q. Guo, W. Shen, M. Li, R. He, Regulating electron density of NiFe-P nanosheets electrocatalysts by a trifle of Ru for high-efficient overall water splitting, Appl. Catal. B: Environ. 263 (2020), 118324.

[5] Y. Zhou, Y. Zhu, X. Yan, Y. Cao, J. Li, B. Dong, M. Yang, Q. Li, C. Liu, Y. Chai, Hierarchical CoSeS nanostructures assisted by Nb doping for enhanced hydrogen evolution reaction, Chin. J. Catal. 42 (2021) 431–438.

[6] X. Zhang, T. Liu, T. Guo, X. Han, Z. Mu, Q. Chen, J. Jiang, J. Yan, J. Yuan, D. Wang, Z. Wu, Z. Kou, Controlling atomic phosphorous-mounting surfaces of ultrafine W_2C nanoislands monodispersed on the carbon frameworks for enhanced hydrogen evolution, Chin. J. Catal. 42 (2021) 1798–1807.

[7] N. Yuan, Q. Jiang, Z. Wu, J. Tang, Ru Nanoparticles decorated on 2D MoO_2 nanosheets as efficient and durable electrocatalysts for the hydrogen evolution reaction in a wide pH range, J. Phys. Chem. C 124 (2020) 10804–10814.

[8] Q. Chen, Y. Nie, M. Ming, G. Fan, Y. Zhang, J. Hu, Sustainable synthesis of supported metal nanocatalysts for electrochemical hydrogen evolution, Chin. J. Catal. 41 (2020) 1791–1811.

[9] Y. Zhou, J. Zhang, H. Ren, Y. Pan, Y. Yan, F. Sun, X. Wang, S. Wang, J. Zhang, Mo doping induced metallic CoSe for enhanced electrocatalytic hydrogen evolution, Appl. Catal. B: Environ. 268 (2020), 118467.

[10] Z. Wu, X. Guo, Z. Zhang, M. Song, T. Jiao, Y. Zhu, J. Wang, X. Liu, Interface engineering of MoS_2 for electrocatalytic performance optimization for hydrogen generation via urea electrolysis, ACS Sustain. Chem. Eng. 7 (2019) 16577–16584.

[11] Q. Liu, E. Wang, G. Sun, Layered transition-metal hydroxides for alkaline hydrogen evolution reaction, Chin. J. Catal. 41 (2020) 574–591.

[12] N. Zang, Z. Wu, J. Wang, W. Jin, Rational design of Cu–Co thiospinel ternary sheet arrays for highly efficient electrocatalytic water splitting, J. Mater. Chem. A 8 (2020) 1799–1807.

[13] M. Cong, D. Sun, L. Zhang, X. Ding, In situ assembly of metal-organic framework-derived N-doped carbon/Co/CoP catalysts on carbon paper for water splitting in alkaline electrolytes, Chin. J. Catal. 41 (2020) 242–248.

[14] C. Fu, X. Yan, L. Yang, S. Shen, L. Luo, G. Wei, J. Zhang, First-principles study of catalytic activity of W-doped cobalt phosphide toward the hydrogen evolution reaction, Chin. J. Catal. 41 (2020) 1698–1705.

[15] L. Yang, L. Huang, Y. Yao, L. Jiao, In-situ construction of lattice-matching NiP_2/$NiSe_2$ heterointerfaces with electron redistribution for boosting overall water splitting, Appl. Catal. B: Environ. 282 (2021), 119584.

[16] H. Yang, X. Chen, G. Hu, W.T. Chen, S.J. Bradley, W. Zhang, G. Verma, T. Nann, D. E. Jiang, P.E. Kruger, X. Wang, H. Tian, G.I.N. Waterhouse, S.G. Telfer, S. Ma, Highly efficient electrocatalytic hydrogen evolution promoted by O-Mo-C interfaces of ultrafine beta-Mo_2C nanostructures, Chem. Sci. 11 (2020) 3523–3530.

[17] M. Cong, D. Sun, L. Zhang, X. Ding, In situ assembly of metal-organic framework-derived N-doped carbon/Co/CoP catalysts on carbon paper for water splitting in alkaline electrolytes, Chin. J. Catal. 41 (2020) 242–248.

[18] Y. Lu, Z. Li, Y. Xu, L. Tang, S. Xu, D. Li, J. Zhu, D. Jiang, Bimetallic Co-Mo nitride nanosheet arrays as high-performance bifunctional electrocatalysts for overall water splitting, Chem. Eng. J. 411 (2021), 128433.

[19] S. Niu, J. Cai, G. Wang, Two-dimensional MoS_2 for hydrogen evolution reaction catalysis: the electronic structure regulation, Nano Res. 14 (2021) 1985–2002.

[20] Y. Song, J. Cheng, J. Liu, Q. Ye, X. Gao, J. Lu, Y. Cheng, Modulating electronic structure of cobalt phosphide porous nanofiber by ruthenium and nickel dual doping for highly-efficiency overall water splitting at high current density, Appl. Catal. B: Environ. 298 (2021), 120488.

[21] S. Guo, Y. Li, S. Tang, Y. Zhang, X. Li, A.J. Sobrido, M.M. Titirici, B. Wei, Monitoring hydrogen evolution reaction intermediates of transition metal dichalcogenides via operando raman spectroscopy, Adv. Funct. Mater. 30 (2020), 2003035.

[22] H. Xu, H. Shang, C. Wang, Y. Du, Ultrafine Pt-based nanowires for advanced catalysis, Adv. Funct. Mater. 30 (2020), 2000793.
[23] L. Chen, Y. Song, Y. Liu, L. Xu, J. Qin, Y. Lei, Y. Tang, NiCoP nanoleaves array for electrocatalytic alkaline H_2 evolution and overall water splitting, J. Energy Chem. 50 (2020) 395–401.
[24] Y. Lei, Y. Wang, Y. Liu, C. Song, Q. Li, D. Wang, Y. Li, Designing atomic active center for hydrogen evolution electrocatalysts, Angew. Chem. Int. Ed. 59 (2020) 20794–20812.
[25] W. Fang, L. Huang, S. Zaman, Z. Wang, Y. Han, B. Xia, Recent progress on two-dimensional electrocatalysis, Chem. Res. Chin. Univ. 36 (2020) 611–621.
[26] C. Xia, Y. Zhou, C. He, A. Douka, W. Guo, K. Qi, B. Xia, Recent advances on electrospun nanomaterials for zinc–air batteries, Small Sci. 1 (2021), 2100010.
[27] J. Wang, Z. Zhang, H. Song, B. Zhang, J. Liu, X. Shai, L. Miao, Water dissociation kinetic-oriented design of nickel sulfides via tailored dual sites for efficient alkaline hydrogen evolution, Adv. Funct. Mater. 31 (2021), 2008578-246.
[28] Y. Liu, X. Li, Q. Zhang, W. Li, Y. Xie, H. Liu, L. Shang, Z. Liu, Z. Chen, L. Gu, Z. Tang, T. Zhang, S. Lu, A general route to prepare low-ruthenium-content bimetallic electrocatalysts for pH-universal hydrogen evolution reaction by using carbon quantum dots, Angew. Chem. Int. Ed. Engl. 59 (2020) 1718–1726.
[29] H. Yoon, H. Song, B. Ju, D. Kim, Cobalt phosphide nanoarrays with crystalline-amorphous hybrid phase for hydrogen production in universal-pH, Nano Res. 13 (2020) 2469–2477.
[30] H. Liu, M. Jin, D. Zhan, J. Wang, X. Cai, Y. Qiu, L. Lai, Stacking faults triggered strain engineering of ZIF-67 derived Ni-Co bimetal phosphide for enhanced overall water splitting, Appl. Catal. B: Environ. 272 (2020), 118951.
[31] C. Wang, X. Shao, J. Pan, J. Hu, X. Xu, Redox bifunctional activities with optical gain of Ni_3S_2 nanosheets edged with MoS_2 for overall water splitting, Appl. Catal. B: Environ. 268 (2020), 118435.
[32] L.F. Hong, R.T. Guo, Y. Yuan, X.Y. Ji, Z.D. Lin, Z.S. Li, W.G. Pan, Recent progress of transition metal phosphides for photocatalytic hydrogen evolution, ChemSusChem 14 (2021) 539–557.
[33] Y. Sun, T. Zhang, C. Li, K. Xu, Y. Li, Compositional engineering of sulfides, phosphides, carbides, nitrides, oxides, and hydroxides for water splitting, J. Mater. Chem. A 8 (2020) 13415–13436.
[34] K. Wang, X. Wang, Z. Li, B. Yang, M. Ling, X. Gao, J. Lu, Q. Shi, L. Lei, G. Wu, Y. Hou, Designing 3d dual transition metal electrocatalysts for oxygen evolution reaction in alkaline electrolyte: beyond oxides, Nano Energy 77 (2020), 105162.
[35] A. Ali, Y. Liu, R. Mo, P. Chen, P.K. Shen, Facile one-step in-situ encapsulation of non-noble metal Co_2P nanoparticles embedded into B, N, P tri-doped carbon nanotubes for efficient hydrogen evolution reaction, Int. J. Hydrogen Energy 45 (2020) 24312–24321.
[36] S. Ramakrishnan, J. Balamurugan, M. Vinothkannan, A.R. Kim, S. Sengodan, D. J. Yoo, Nitrogen-doped graphene encapsulated FeCoMoS nanoparticles as advanced trifunctional catalyst for water splitting devices and zinc–air batteries, Appl. Catal. B: Environ. 279 (2020), 119381.
[37] Y. Zhao, Y. Gao, Z. Chen, Z. Li, T. Ma, Z. Wu, L. Wang, Trifle Pt coupled with NiFe hydroxide synthesized via corrosion engineering to boost the cleavage of water molecule for alkaline water-splitting, Appl. Catal. B: Environ. 297 (2021), 120395.
[38] H. Xua, H. Jia, B. Fei, Y. Ha, H. Li, Y. Guo, M. Liu, R. Wu, Charge transfer engineering via multiple heteroatom doping in dual carbon-coupled cobalt phosphides for highly efficient overall water splitting, Appl. Catal. B: Environ. 268 (2020), 118404.
[39] M. Cong, D. Sun, L. Zhang, X. Ding, In situ assembly of metal-organic framework-derived N-doped carbon/Co/CoP catalysts on carbon paper for water splitting in alkaline electrolytes, Chin. J. Catal. 41 (2020) 242–248.
[40] L. Zhang, X. Hao, J. Li, Y. Wang, Z. Jin, Unique synergistic effects of ZIF-9(Co)-derived cobalt phosphide and $CeVO_4$ heterojunction for efficient hydrogen evolution, Chin. J. Catal. 41 (2020) 82–94.
[41] L. Zhang, W. Xiao, Y. Zhang, F. Han, X. Yang, Nanocarbon encapsulating Ni-doped MoP/graphene composites for highly improved electrocatalytic hydrogen evolution reaction, Compos. Commun. 26 (2021), 100792.
[42] M. Li, H. Li, X. Jiang, M. Jiang, X. Zhan, G. Fu, J.-M. Lee, Y. Tang, Gd-induced electronic structure engineering of a NiFe-layered double hydroxide for efficient oxygen evolution, J. Mater. Chem. A 9 (2021) 2999–3006.
[43] G. Zhou, M. Li, Y. Li, H. Dong, D. Sun, X. Liu, L. Xu, Z. Tian, Y. Tang, Regulating the electronic structure of CoP nanosheets by O incorporation for high-efficiency electrochemical overall water splitting, Adv. Funct. Mater. 30 (2019), 1905252.
[44] C. Chen, W. Luo, H. Li, T. Hu, Y. Zhao, Z. Zhao, X. Sun, H. Zai, Y. Qi, M. Wu, Y. Dong, J. Dong, W. Chen, X. Ke, M. Sui, L. Zhang, Q. Chen, Z. Wang, E. Zhu, Y. Li, Y. Huang, Optimized MoP with pseudo-single-atom tungsten for efficient hydrogen electrocatalysis, Chem. Mater. 33 (2021) 3639–3649.
[45] Y. Men, P. Li, J. Zhou, S. Chen, W. Luo, Trends in alkaline hydrogen evolution activity on cobalt phosphide electrocatalysts doped with transition metals, Cell Rep. Phys. Sci. 1 (2020), 100136.
[46] Y. Gu, A. Wu, Y. Jiao, H. Zheng, X. Wang, Y. Xie, L. Wang, C. Tian, H. Fu, Two-dimensional porous molybdenum phosphide/nitride heterojunction nanosheets for pH-universal hydrogen evolution reaction, Angew. Chem. Int. Ed. 60 (2021) 6673–6681.
[47] J. Chen, H. Wang, Y. Gong, Y. Wang, Directly immobilizing a Ru–tannic acid linkage coordination complex on carbon cloth: an efficient and ultrastable catalyst for the hydrogen evolution reaction, J. Mater. Chem. A 7 (2019) 11038–11043.
[48] A. Annamalai, D.V. Shinde, J. Buha, S. Marras, M. Prato, S. Lauciello, L.D. Trizio, L. Manna, Synthesis of yolk–shell $Co_3O_4/Co_{1-x}Ru_xO_2$ microspheres featuring an enhanced electrocatalytic oxygen evolution activity in acidic medium, J. Mater. Chem. A 9 (2021) 10385–10392.
[49] J. Zhang, M. Song, J. Wang, Z. Wu, X. Liu, In-situ transformation to accordion-like core-shell structured metal@metallic hydroxide nanosheet from nanorod morphology for overall water-splitting in alkaline media, J. Colloid Interfaces Sci. 559 (2020) 105–114.
[50] M. Song, Y. Zhao, Z. Wu, X. Liu, MoS_2/CoB with Se doping on carbon cloth to drive overall water-splitting in an alkaline electrolyte, Sustain. Energy Fuels 4 (2020) 5036–5041.
[51] Y. Li, F. Chu, Y. Bu, Y. Kong, Y. Tao, X. Zhou, H. Yu, J. Yu, L. Tang, Y. Qin, Controllable fabrication of uniform ruthenium phosphide nanocrystals for the hydrogen evolution reaction, Chem. Commun. 55 (2019) 7828–7831.
[52] D. Zheng, C. Lv, X. Zhang, S. Chen, H. Liu, Y. Sun, X. She, D. Yang, Activation of interfacial P sites of CoP in RuP_3/CoP nanosheets boosts hydrogen evolution reaction at all pH values, Mater. Today 13 (2021), 100074.
[53] C. Chen, W. Luo, H. Li, T. Hu, Y. Zhao, Z. Zhao, X. Sun, H. Zai, Y. Qi, M. Wu, Y. Dong, J. Dong, W. Chen, X. Ke, M. Sui, L. Zhang, Q. Chen, Z. Wang, E. Zhu, Y. Li, Y. Huang, Optimized MoP with pseudo-single-atom tungsten for efficient hydrogen electrocatalysis, Chem. Mater. 33 (2021) 3639–3649.
[54] L. Yu, J. Zhang, Y. Dang, J. He, Z. Tobin, P. Kerns, Y. Dou, Y. Jiang, Y. He, S.L. Suib, In situ growth of Ni_2P–Cu_3P bimetallic phosphide with bicontinuous structure on self-supported NiCuC substrate as an efficient hydrogen evolution reaction electrocatalyst, ACS Catal. 9 (2019) 6919–6928.
[55] Q. Cao, S. Hao, Y. Wu, K. Pei, W. You, R. Che, Interfacial charge redistribution in interconnected network of Ni_2P–Co_2P boosting electrocatalytic hydrogen evolution in both acidic and alkaline conditions, Chem. Eng. J. 424 (2021), 130444.
[56] J.-S. Li, J.-Y. Li, M.-J. Huang, L.-X. Kong, Z. Wu, Anchoring Ru_xP on 3D hollow graphene nanospheres as efficient and pH-universal electrocatalysts for the hydrogen evolution reaction, Carbon 161 (2020) 44–50.
[57] C. Chen, W. Luo, H. Li, T. Hu, Y. Zhao, Z. Zhao, X. Sun, H. Zai, Y. Qi, M. Wu, Y. Dong, J. Dong, W. Chen, X. Ke, M. Sui, L. Zhang, Q. Chen, Z. Wang, E. Zhu, Y. Li, Y. Huang, Optimized MoP with pseudo-single-atom tungsten for efficient hydrogen electrocatalysis, Chem. Mater. 33 (2021) 3639–3649.
[58] L. Wang, J. Fan, Y. Liu, M. Chen, Y. Lin, H. Bi, B. Liu, N. Shi, D. Xu, J. Bao, M. Han, Phase-modulation of iron/nickel phosphides nanocrystals “armored” with porous P-doped carbon and anchored on P-doped graphene nanohybrids for enhanced overall water splitting, Adv. Funct. Mater. 31 (2021), 2010912.
[59] Z. Wu, D. Nie, M. Song, T. Jiao, G. Fu, X. Liu, Facile synthesis of Co–Fe–B–P nanochains as an efficient bifunctional electrocatalyst for overall water-splitting, Nanoscale 11 (2019) 7506–7512.
[60] C. Chen, W. Luo, H. Li, T. Hu, Y. Zhao, Z. Zhao, X. Sun, H. Zai, Y. Qi, M. Wu, Y. Dong, J. Dong, W. Chen, X. Ke, M. Sui, L. Zhang, Q. Chen, Z. Wang, E. Zhu, Y. Li, Y. Huang, Optimized MoP with pseudo-single-atom tungsten for efficient hydrogen electrocatalysis, Chem. Mater. 33 (2021) 3639–3649.
[61] M. Song, Z. Zhang, Q. Li, W. Jin, Z. Wu, G. Fu, X. Liu, Ni-foam supported Co(OH)F and Co–P nanoarrays for energy-efficient hydrogen production via urea electrolysis, J. Mater. Chem. A 7 (2019) 3697–3703.
[62] W. Zhou, M. Wu, G. Li, Rambutan-like CoP@Mo-Co-O hollow microspheres for efficient hydrogen evolution reaction in alkaline solution, Chin. J. Catal. 41 (2020) 691–697.
[63] H. Xu, Q. Jiang, B. Zhang, C. Chen, Z. Lin, Integrating conductivity, immobility, and catalytic ability into high-N carbon/graphene sheets as an effective sulfur host, Adv. Mater. 32 (2020), 1906357.
[64] S. Muratsugu, A. Yamaguchi, G.I. Yokota, T. Maeno, M. Tada, Tuning the structure and catalytic activity of Ru nanoparticle catalysts by single 3d transition-metal atoms in Ru_{12}-metalloporphyrin precursors, Chem. Commun. 54 (2018) 4842–4845.